Sensors and Materials, Vol. 21, No. 5 (2009) 265–280
MYU Tokyo

S & M 0767

Chemical Modification of Carbon Nanotubes for NO_2 Detection

Takeshi Hashishin* and Jun Tamaki

College of Life Sciences, Department of Applied Chemistry, Ritsumeikan University,
1-1-1 Nojihigashi, Kusatsu, Shiga 525-8577, Japan

(Received April 6, 2009; accepted June 2, 2009)

Key words: carbon nanotubes, oxides, chemical modification, NO_2, p-n junction

Multiwalled carbon nanotubes (MWNTs) were oxidized by nitric acid in order to simultaneously induce defects and hydrophilic (carboxyl) groups on the surface of MWNTs, on the basis of the concept that defects and carboxyl groups could contribute to the increase in the number of adsorption sites of gas molecules such as NO_2. It was observed by transmission electron microscope (TEM) that oxidized MWNTs had a rough sidewall surface. The sensor response to dilute NO_2 (R_a/R_g) of an oxidized MWNT-based sensor was 50% higher than that of an as-grown MWNT-based sensor, suggesting an increase in the number of NO_2 adsorption sites with an increase in the density of defects on the surface of MWNTs. On the other hand, the p-n junction of a semiconductor generally contributes to increasing electric resistance by forming a space charge layer. A space charge layer could be expected to enhance NO_2 gas adsorption. Thus, MWNTs as p-type semiconductors were modified with an n-type semiconductor such as WO_3 and SnO_2 nanoparticles, which generally exhibit an excellent sensor response to dilute NO_2. MWNT-WO_3 and MWNT-SnO_2 composite sensors showed a fairly good sensor response (R_a/R_g) to dilute NO_2, compared with that of the MWNT-based sensor. The addition of an n-type oxide to MWNTs contributes to the formation of a large depletion layer within MWNTs by the p-n junction on contact points between MWNTs and oxides, resulting in an increase in resistance in air and the enhancement of NO_2 adsorption.

1. Introduction

Carbon nanotubes (CNTs) are one of the new candidate materials for a variety of potential applications.[1] Recently, CNT-based gas sensors have received considerable attention because of their excellent properties, such as faster response, higher sensitivity, and lower operating temperature for the detection of gases such as NO_2 and NH_3.[2–8] To enhance their sensitivity to air pollution gases, it is more effective that CNTs are chemically oxidized by acid solutions such as nitric and sulfuric acids in order to generate gas adsorption sites as carboxyl groups and carbonyl on the surface of CNTs[9–17]

*Corresponding author: e-mail: hasisin@sk.ritsumei.ac.jp

and that CNTs are modified with metallic particles of Au,[18] Pt[19] or oxides such as SnO_2, WO_3, and TiO_2.[20] Interestingly, Au or Pt nanoparticles deposited on multiwalled carbon nanotubes (MWNTs) behave as p-type semiconductors when exposed to NO_2 and NH_3.[18,19] In the case of the MWNT-oxide composite gas sensor,[20] the enhancement of gas sensitivity depends on the formation of a p-n junction at the surface of the main matrix with either oxides or nanotubes when oxygen in air negatively adsorbs on the surface.

This work is on the NO_2 sensing properties of a pristine MWNT-based gas sensor and three types of MWNT-based gas sensor: (1) MWNTs were oxidized using a "wet" chemistry process such as nitric acid treatment to introduce defects on the aromatic ring of carbon nanotubes leading to an increase in the number of gas adsorption sites; (2) the surfaces of MWNTs were modified with disklike WO_3 small grains 300 nm in diameter and 50 nm in thickness to improve sensor response to 5 ppm NO_2 and discuss the interaction between MWNTs and WO_3 when the amount of WO_3 added to MWNTs is varied; (3) the sensing properties of a MWNT-SnO_2 composite sensor to 1 ppm NO_2 were investigated for three deposition states of SnO_2 nanoparticles inside/outside MWNTs.

2. Experimental Procedure

2.1 *MWNT-based sensor*

Microgap electrodes with various gap sizes were fabricated by MEMS techniques. A Au line with a width of 20 μm, a gap size of 5 μm, and a thickness of 0.3 μm was formed on a SiO_2 substrate by photolithography (lift off), as shown in Fig. 1. A growth catalyst

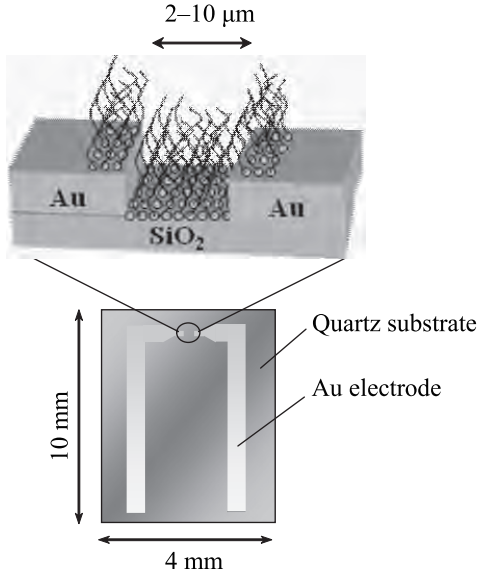

Fig. 1. Schematic diagram of MWNT-based sensor.

of 0.05 wt% $Ni(CH_3COO)_2$ aqueous solution was dropped on a Au electrode with a 5 μm gap using a microinjector, and dried at room temperature for 30 min to serve as a Ni-deposited substrate. This substrate was subsequently set on the electric furnace, and MWNTs were directly grown at the microgap of Au at 625 to 700°C for 60 min using a nickel catalyst in a gas mixture of ethanol, argon, and hydrogen (6 kPa).

2.2 *Oxidized MWNT-based sensor*

An aqueous solution of nitric acid (1 mol/L) was dropped on the MWNT-based sensor using a microinjector, and dried at 100°C for 15 min, in order to clarify the difference in sensing properties between raw and oxidized MWNTs.

2.3 *MWNT-WO_3 composite sensor*

The WO_3 powder was prepared from $(NH_4)_{10}W_{12}O_{41}\cdot 5H_2O$ by a wet process. An aqueous solution of $(NH_4)_{10}W_{12}O_{41}\cdot 5H_2O$ was neutralized using dilute nitric acid solution. The precipitate obtained (H_2WO_4) was thoroughly washed with deionized water, dried, and dispersed in deionized water to form a suspension. A microdrop of suspension ranging from 0.1 to 7 wt% H_2WO_4 was directly dropped on the surface of the MWNTs grown between Au electrodes with a microgap (5 μm) by microinjection, dried, and calcined at 400°C for 3 h in an inert gas of argon to prevent the oxidation of MWNTs. The MWNT-WO_3 composite sensor obtained by dropping the suspension of 0.1 wt% H_2WO_4 on an MWNT-based sensor is hereafter expressed as the MWNT-0.1 wt% WO_3 sensor.

2.4 *MWNT-SnO_2 composite sensor*

Growth catalysts of MWNTs such as nickel should be removed from inside MWNTs in order to fill them with oxides. It is also desired that MWNTs have a uniform G/D ratio for reproducibility of filling MWNTs with a tin source such as $SnCl_2$. The details of the G/D ratio of MWNTs are explained in § 2.5. The MWNTs were purchased from Wako Pure Chemical Industries, Ltd. They were oxidized using concentrated nitric acid to open the tip edges of the MWNTs and to remove the growth catalysts and amorphous carbon. TEM of the oxidized MWNTs showed that the MWNTs were 20–50 nm in diameter and 5–50 μm in length. Raman spectroscopy showed that the MWNTs have a G/D ratio of more than 1.5 even after oxidization. MWNT-SnO_2 composites were prepared by two methods. The oxidized MWNTs were immersed in 0.1 wt% $SnCl_2$ aqueous solution, which was stirred at R. T. for 20 h to introduce the Sn component into the MWNTs. Tin oxides and those deposited inside/outside MWNTs were separated by centrifugation after drying at 120°C for 3 h in air to induce Sn component oxidation. Excess SnO_2 deposited outside the MWNTs was removed using deionized water and dried at 35°C for 2 h in air. Finally, SnO_2-deposited MWNTs were calcined at 400°C for 3 h in air or 600°C for 3 h in argon in order to control the deposition state of SnO_2 particles inside/outside MWNTs.

2.5 *Characterization of MWNTs*

Two main features in the Raman spectra of MWNTs are generally the D- and G-peaks at about 1350 and 1600 cm^{-1}, respectively. The G-band corresponds to the

symmetric E_{2g} vibrational mode in graphitelike materials, while the D-band is activated in the first-order scattering process of sp^2 carbons by the presence of substitutional heteroatoms, vacancies, or other defects, all of which are consistent with disordered graphitic bonding within the tubes. The relative peak intensity ratio of the G-band to the D-band in Raman shift of pristine or oxidized MWNTs was measured by Raman spectroscopy (Nanofinder30, Tokyo Instruments) in order to investigate the correlation between the amount of defective sites on the surface of MWNTs and that of NO_2 adsorption. The morphology and microstructure of a raw MWNT, an oxidized MWNT and an MWNT-oxide composite were observed by field-emission scanning electron microscopy (FE-SEM, Hitachi S-4800) and transmission electron microscopy (TEM, JEOL JEM-2010), respectively. Fourier transform infrared spectroscopy (FT-IR, Shimazu IR Affinity-1) was used to confirm the surface states of oxidized MWNTs.

2.6 *Evaluation of sensing properties to dilute NO_2*

The three types of MWNT-based sensor obtained at various growth temperatures were placed in a flow apparatus equipped with an electric furnace and the sensing properties to dilute NO_2 (5 ppm) were measured at R. T. and 100 to 250°C every 50°C. A NO_2 (10.6 ppm) + N_2 high-pressure gas tank was used for the preparation of 5 ppm NO_2. The sensor response ($S = R_a/R_g$) was defined as the ratio of resistance in air atmosphere (R_a) to that in NO_2-containing air atmosphere (R_g). In the case of the MWNT-WO_3 composite sensor, the optimum operating temperature was determined to be 200°C by investigating the preliminary conductive behaviors of WO_3 and MWNTs to 5 ppm NO_2. The sensing property of the MWNT-SnO_2 composite sensor to 1 ppm NO_2 was examined in the temperature range from 100 to 250°C in order to measure resistance change when exposed to 1 ppm NO_2. Resistance change (%) was defined as $((R_g-R_a)/R_a)\times100$ in the evaluation of the MWNT-SnO_2 composite sensor.

3. Results and Discussion

3.1 *MWNT-based sensor*

A high-resolution field-emission electron scanning microscopy (HR-FE-SEM) image of MWNTs deposited between Au electrodes at 700°C for 60 min via ethanol CVD is shown in Fig. 2, corresponding to the circular area in Fig. 1. This image shows nanotubes with a diameter range of 5-20 nm, and entangled and aligned carbon nanotubes with a metal cap predominantly located on their top.

The MWNT-based sensors obtained at 625, 650, and 700°C were exposed to 5 ppm NO_2 for 10 min after R_a was stabilized at an operating temperature of 100°C for 3 min. Air flowed to the sensor immediately after the flow of 5 ppm NO_2 was turned off. The response transients to 5 ppm NO_2 are shown in Fig. 3. These responses indicated that the MWNT-based sensor behaved as a p-type semiconductor because the resistance became lower in NO_2-containing atmosphere. The electric resistances of the MWNTs obtained at 625 and 650°C were higher than those of the MWNTs obtained at 700°C. The response-recovery characteristics became sluggish with decreasing growth temperature of MWNTs immediately after each MWNT was exposed to NO_2. On the other hand, the sensor

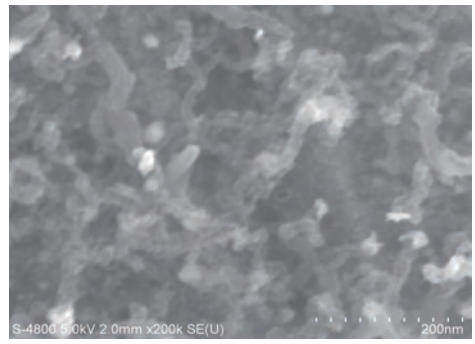

Fig. 2. SEM images of the 10-μm-gap area of the MWNT-based sensor directly grown for 1 h at 700°C via ethanol CVD.

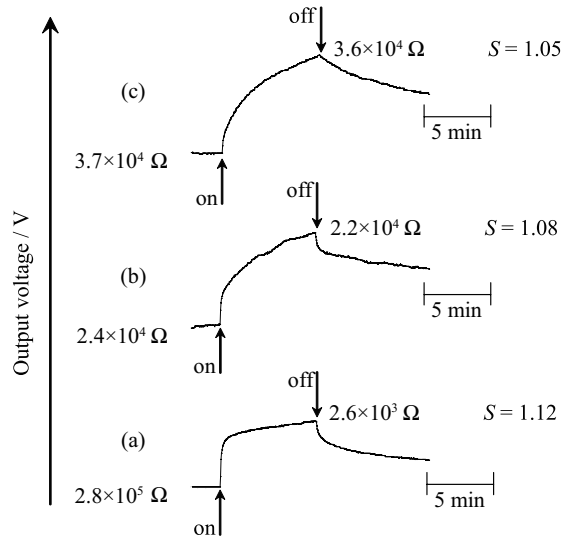

Fig. 3. Response transients of MWNT sensors to 5 ppm NO_2 in air at 100°C, which were grown for 1 h at (a) 625, (b) 650, and (c) 700°C via ethanol CVD.

response (S) of MWNTs grown at low temperatures was higher than that of MWNTs grown at high temperatures. These tendencies suggest that the crystallinity of MWNTs is related to sensor response.

The Raman spectra of the MWNT-based gas sensor fabricated at 625, 650, 700 and 750°C are shown in Fig. 4. The peak intensity ratio of the G-band to the D-band increased with increasing growth temperature of MWNTs. We investigated the effects of growth temperature on the resistance in air or sensor response to NO_2 adsorption on MWNTs, as shown in Figs. 5(a) and 5(b), respectively. The sensor response of the MWNT-based sensor fabricated at 750°C was almost unity. This means that NO_2

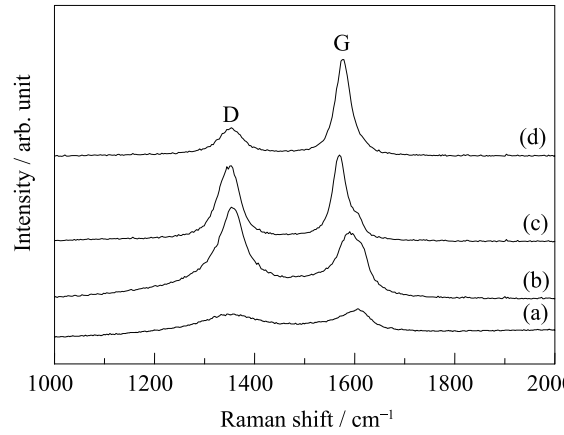

Fig. 4. Raman spectra of MWNT sensors grown for 1 h at (a) 625, (b) 650, (c) 700, and (d) 750°C via ethanol CVD.

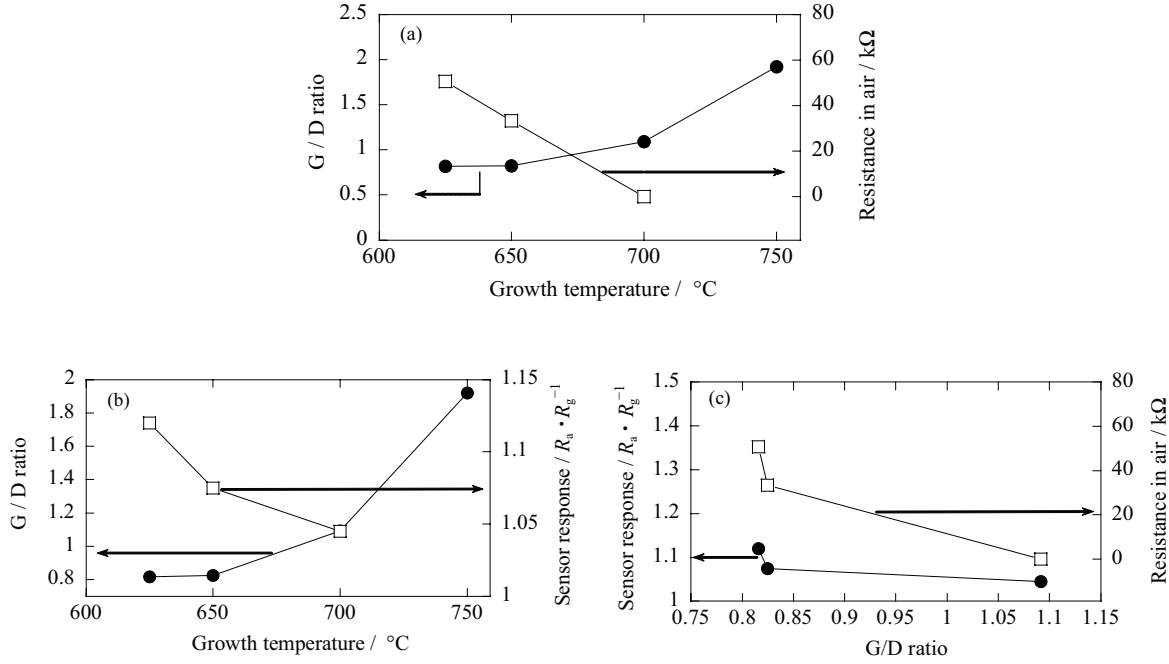

Fig. 5. Effects of growth temperature on (a) resistance in air and (b) sensor response of MWNT-based sensor to 5 ppm NO_2 at 100°C, and (c) dependence of resistance in air and sensor response on the G/D ratio of Raman shift of MWNTs.

gas did not adsorb on the surface of individual MWNTs between Au electrodes. The sensor response of the MWNT-based sensor fabricated at 700°C tended to be low at all operating temperatures, compared with those of the MWNT-based sensors fabricated at 625 and 650°C. These behaviors seem to relate to the amount of defective sites on the surface of MWNTs. The resistance in air (R_a) and sensor response (R_a/R_g) of the MWNT-based sensor decreased with increasing growth temperature. This behavior is considered to be consistent with general semiconductive properties, i.e., electric resistance decreases with increasing operating temperature. On the other hand, the resistance in air and sensor response decreased with increasing G/D ratio, as shown in Fig. 5(c). The electrical properties of thin films of MWNTs can be tuned by adjusting the deposition temperature, and a transition from a defective structure to a defect-free structure can be induced through high-temperature exposure to reactive plasma in order to control the defective sites on the side wall of MWNTs.[4] Valentini described that the interaction of the adsorbed NO_2 molecules with MWNT defective sites is enhanced, whereas NO_2 does not chemically interact with the sidewall of the tubes grown at a higher deposition temperature. Therefore, from the results in Fig. 5(c), NO_2 molecules were considered to adsorb to defective sites on the sidewall of MWNTs with a lower G/D ratio in Raman spectra, grown at 625°C, leading to higher electrical resistance and better sensor response.

The response of an MWNT-based gas sensor at each growth temperature to 5 ppm NO_2 as a function of operating temperature is shown in Fig. 6. The MWNT-based sensor obtained at 700°C indicated almost the same sensor response at all operating temperatures. It is suggested that the number of defective sites on the side wall of MWNTs corresponds to the amount of NO_2 adsorption. In contrast, the sensor responses of MWNTs grown at 625 and 650°C tended to decrease with increasing operating

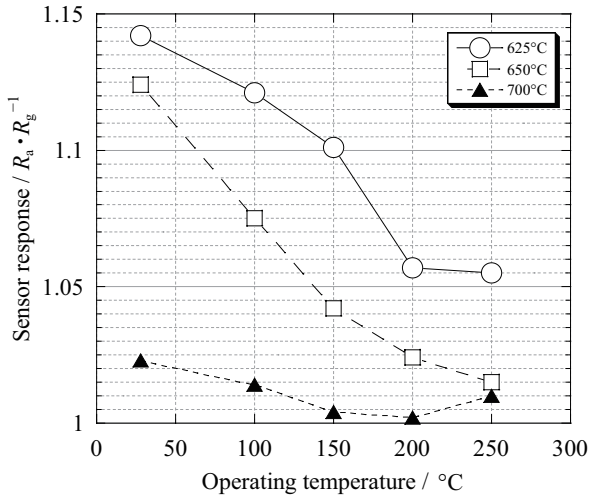

Fig. 6. Responses of MWNT-based sensors fabricated at growth temperatures of 625, 650, and 700°C to 5 ppm NO_2 as a function of operating temperature.

temperature. This tendency indicates that the MWNTs have general semiconductive behavior. The MWNTs obtained at lower growth temperatures such as 625 and 650°C would have many defective sites on their sidewalls. Therefore, the number of defective sites on their sidewalls can be controlled by the growth temperature of MWNTs, inducing an increase in the amount of NO_2 adsorption.

3.2 *Oxidized MWNT-based sensor*

The effect of oxidation of MWNTs is summarized in Fig. 7. The sensor response of an oxidized MWNT-based sensor to 5 ppm NO_2 was higher than that of a raw MWNT-based sensor, as shown in Fig. 7(a). This tendency was related to the surface state

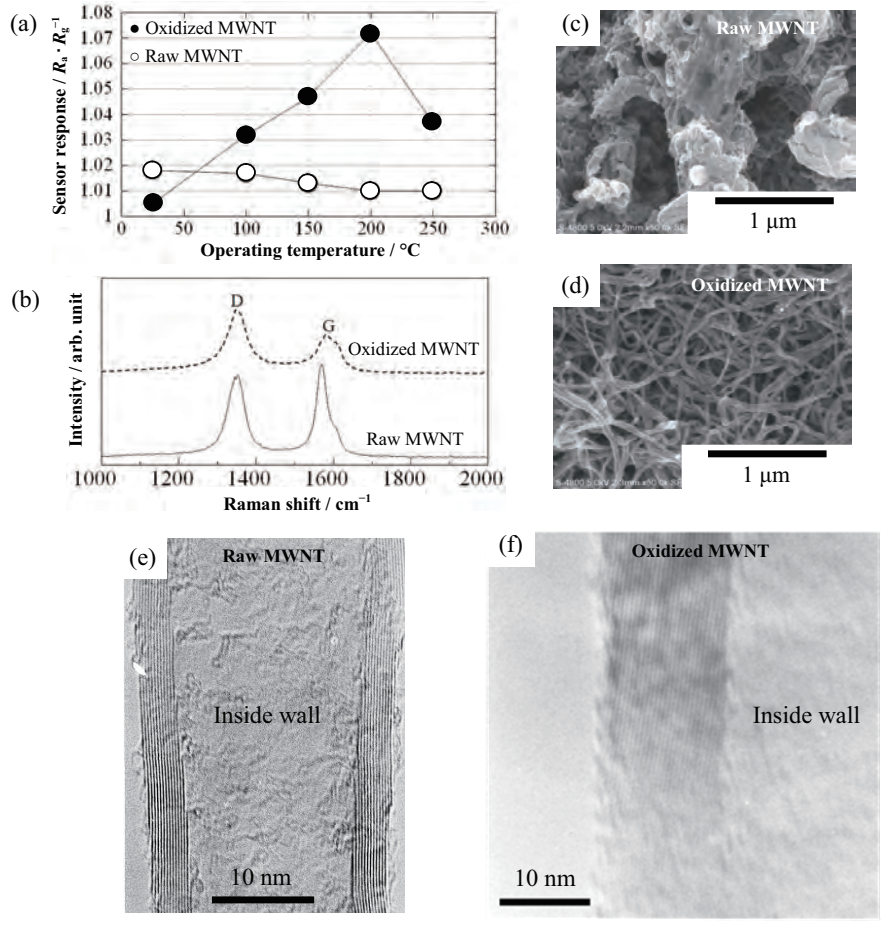

Fig. 7. Oxidation effects of MWNT on (a) sensor response to 5 ppm NO_2 as a function of operating temperature, (b) intensity of the G-band and the D-band in Raman spectra, (c, d) surface morphologies, and (e, f) roughness of sidewall.

of MWNTs changed by the nitric oxidation, as seen in the ratio of the G-band to the D-band for Raman spectra with or without the nitric oxidation in Fig. 7(b). SEM images of Figs. 7(c) and 7(d) respectively show the raw and oxidized MWNTs. The surface morphologies of raw and oxidized MWNTs were different and a particularly smooth surface was formed by nitric oxidation, suggesting the elimination of amorphous carbon aggregated on the surface of MWNTs. Figures 7(e) and 7(f) respectively indicate the high-resolution images of lamination carbon layers for the side wall of MWNTs with and without nitric oxidation. The outside wall of the oxidized MWNTs clearly indicates an ambiguous edge and an unclear stacking carbon layer compared with that of raw MWNTs. Namely, nitric oxidation seems to remove amorphous and introduce carboxyl groups on the outside surface of MWNTs. The infrared absorption spectra of MWNTs with and without oxidation are shown in Fig. 8. The oxidized MWNTs were assigned to the stretching vibrations of C-O, C=O and COO- at respective wave numbers of 1100–1200, 1650–1740 and 1320–1550 cm^{-1} in addition to 1578 cm^{-1} of aromatic C-C related to the graphene sheet of MWNTs. It seems that these hydrophilic groups contribute to the adsorption of NO_2 enhancing the increase in sensor response, although we have unfortunately no evidence of the chemical affinity between carboxyl groups and NO_2 adsorption.

3.3 *MWNT-WO_3 composite sensor*

MWNTs 20–50 nm in diameter, which were grown at 700°C for 60 min in a gas mixture of ethanol, argon, and H_2 (6 kPa), have an entangled shape, as shown in Figs. 9(a) and 9(b). Microstructural analysis using Raman techniques and TEM indicated that the ratio of the G-band to the D-band was closest to 1. The entangled MWNTs formed a network structure with each other (Fig. 9(b)).

SEM images of MWNT-WO_3 composites with various WO_3 amounts are shown in Fig. 10. In the MWNT-0.1 wt% WO_3 composite, WO_3 grains were independently trapped and MWNTs were clearly observed as shown in Fig. 10(a). The grain sizes of

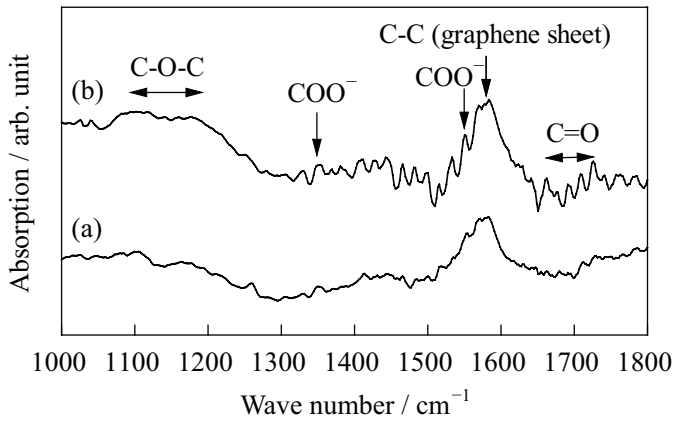

Fig. 8. Infrared absorption spectra of (a) MWNT and (b) oxidized MWNT.

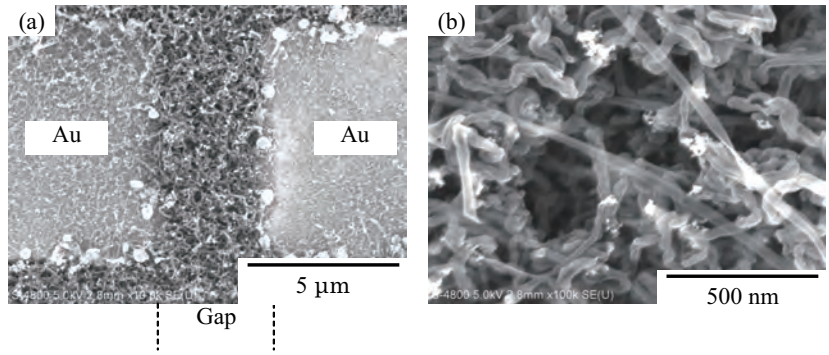

Fig. 9. SEM image of (a) MWNTs directly grown on Au microgap and magnified image of (b) entangled MWNTs between Au electrodes.

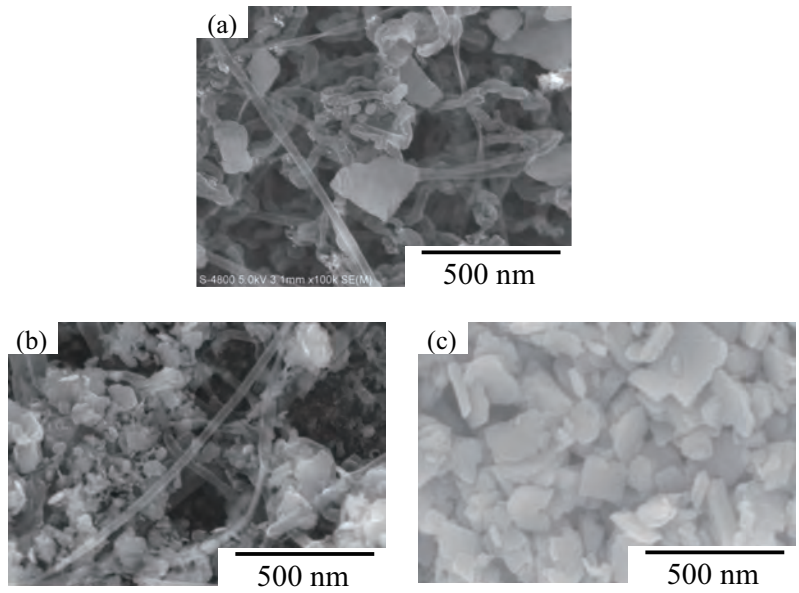

Fig. 10. SEM images of MWNT-WO_3 composite sensors obtained by argon calcination of MWNT-based sensor to which (a) 0.1, (b) 1 and (c) 7 wt% H_2WO_4 suspensions were added.

WO_3 trapped on MWNTs ranged from 50 to 200 nm and the grains were almost disklike or plateletlike. With increasing WO_3 amount, as shown in Figs. 10(b) and 10(c), the number of WO_3 grains increased and MWNTs became less visible, suggesting the formation of WO_3 connections.

Figure 11 shows the response transients of MWNT and MWNT-WO_3 sensors to 5 ppm NO_2 at 200°C. The resistances of both MWNT and MWNT-WO_3 sensors decreased upon exposure to NO_2, suggesting that conduction occurs through p-type MWNTs in both MWNT and MWNT-WO_3 sensors. The sensor response (R_a/R_g) of the MWNT-0.1 wt% WO_3 sensor was as high as 3.8; however, the MWNT sensor showed almost no response (R_a/R_g = 1.05).

Figure 12 shows the resistance in air and the sensor response of the MWNT-WO_3 composite as a function of the additional amount of H_2WO_4 suspension. The resistance markedly increased at 0.1 wt% H_2WO_4 addition. After reaching the maximum value of resistance, the resistance gradually decreased with increasing additional amount of H_2WO_4. This behavior can be explained by the formation of a p-n junction at 0.1 wt% and the many connection sites of each WO_3 particle at higher than 1 wt%. A similar behavior was observed for the sensor response, which had a maximum at 0.1 wt%. At

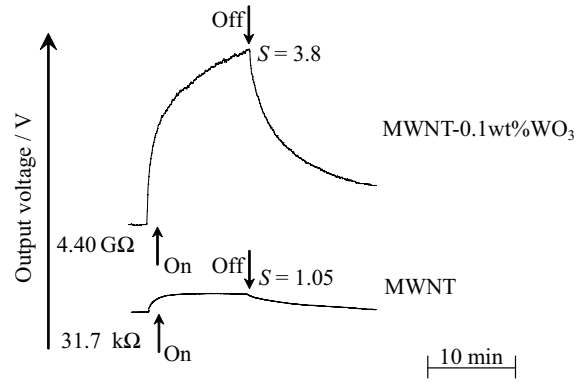

Fig. 11. Response transients of MWNT and MWNT-0.1 wt% WO_3 composite sensors to 5 ppm NO_2 at 200°C.

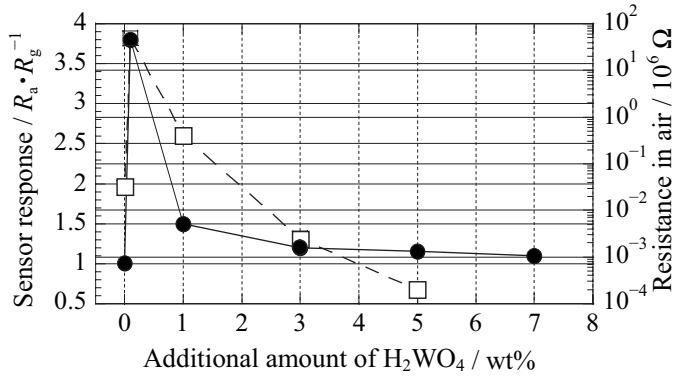

Fig. 12. Sensor response and resistance in air of MWNT-WO_3 composite sensors as a function of additional amount of H_2WO_4. (● Sensor response and □ Resistance in air)

0.1 wt%, a p-n junction was formed between the MWNTs and WO_3 grains to generate a large depletion layer within the MWNTs, inducing a large resistance in the MWNT-WO_3 composite sensor. The highly depleted surface state of MWNTs resulted in an increasing amount of NO_2 adsorbed on the MWNT, and thus a high sensor response of the MWNT-WO_3 composite sensor to dilute NO_2. At higher than 1 wt%, the conduction pass was formed through WO_3 grains to decrease sensor resistance. At higher than 1 wt% WO_3, the WO_3 grains come into contact with each other for a dominant n-type conductive pass owing to WO_3. WO_3 is an excellent sensing material for NO_2 detection. Although the WO_3 sensor shows a resistance increase as a response, the MWNT-WO_3 (7 wt%) composite sensor exhibited no response to 5 ppm NO_2 (R_a/R_g = 1). It is considered that the sensor response (R_a/R_g) would be decreased to less than unity (resistance increase) at a higher amount of WO_3. Finally, the reproducibility of the sensor response to 5 ppm NO_2 was examined at 200°C for MWNT-0.1 and 1 wt% WO_3 composites. As a result, the sensor responses of the composites were respectively 3.6 and 1.4, which were close to the plotted data of Fig. 12.

3.4 *MWNT-SnO_2 composite sensor*

Well-dispersed SnO_2 nanoparticles a few nanometers in diameter deposited inside the MWNTs were prepared by calcination at 400°C for 3 h in air after washing with deionized water, as shown in Fig. 13(a). On the other hand, in the case without washing with deionized water, Fig. 13(b) shows the MWNTs fully covered with SnO_2

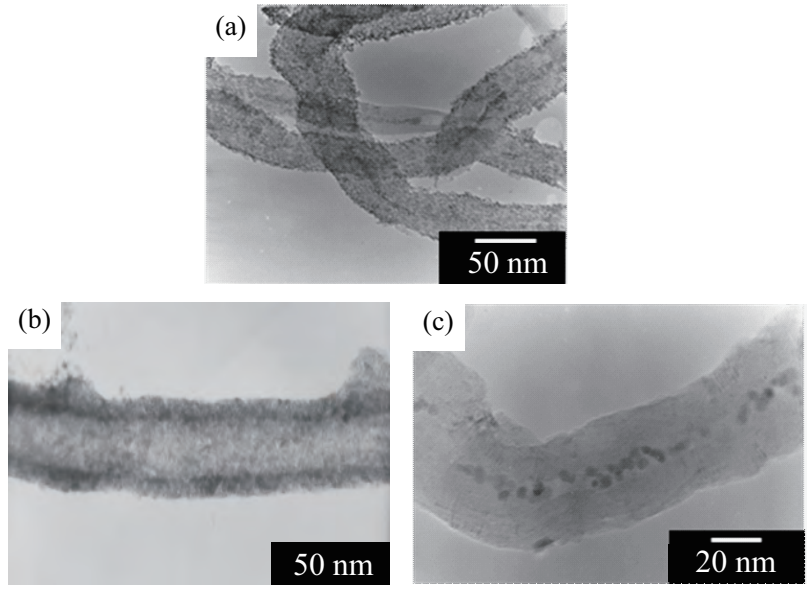

Fig. 13. TEM images of MWNT-SnO_2 composite fabricated by (a) calcination at 400°C for 3 h in air after washing with deionized water, (b) calcination at 400°C for 3 h in air and (c) calcination at 600°C for 3 h in argon and at 400°C for 3 h in air.

nanoparticles of more than 5 nm in diameter. Interestingly, SnO_2 nanoparticles deposited outside the MWNTs were removed and the nanoparticles inside the MWNTs became 10 nm in diameter with calcination at 600°C for 3 h under a flow of argon and subsequent heat treatment at 400°C for 3 h in air, as shown in Fig. 13(c). The SnO_2 nanoparticles deposited inside the MWNTs indicated either 110 or 101 lattice fringes, which are in accordance with the cassiterite SnO_2 lattice fringe spacing given as 0.335 and 0.268 nm from TEM, respectively. During heat treatment in air, the inner nanoparticles were crystallized and grew larger. The growth of SnO_2 particles is restricted by the size of the inner diameter of MWNTs. The calcination of SnO_2 nanoparticles deposited inside/outside MWNTs in a stream of argon can repair the carbon defects on the surface of MWNTs. It was very difficult to distinguish the relative difference in intensity between the D-band of raw MWNTs and that of oxidized MWNTs because MWNTs have many defective sites on their surfaces. In order to clearly confirm the increase in the D-band intensity with nitric oxidation, single-walled carbon nanotubes (SWNTs) purchased from SES Research Inc. were oxidized using concentrated nitric acid. Raman spectra of raw and oxidized SWNTs are shown in Figs. 14(a) and 14(b), respectively. The intensity of the D-band was increased in the Raman spectrum of oxidized SWNTs compared with that of raw SWNTs, suggesting an increase in the number of defective sites on the surface of oxidized SWNTs. On the other hand, the calcination of SWNTs in argon led to a decrease in the intensity of the D-band, as shown in Fig. 14(c). Thus, it is suggested that carboxyl groups as adsorbates of SnO_2 nanoparticles on the carbon defects disappear during calcination in argon and nanoparticles are removed from the outer surface of MWNTs.

The response transients of the oxidized MWNTs obtained by nitric oxidation and two SnO_2-MWNT composites to 1 ppm NO_2 at an operating temperature of 150°C are shown

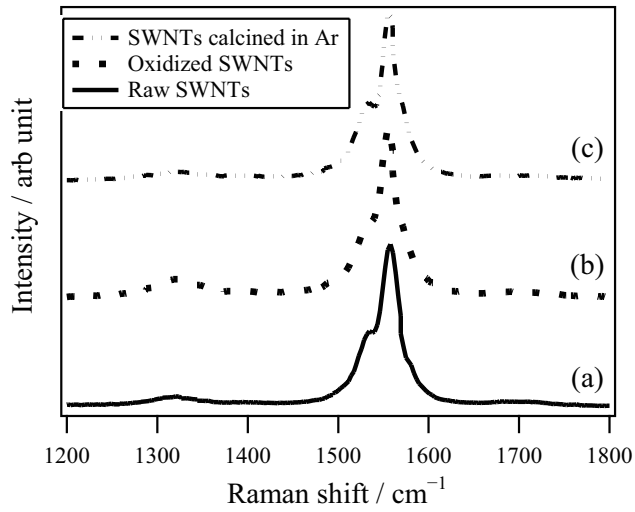

Fig. 14. Raman spectra of (a) raw SWNTs, (b) oxidized SWNTs and (c) SWNTs calcined at 600°C for 3 h in argon.

in Fig. 15. The resistance in air of these sensors at each operating temperature is plotted in Fig. 16. The oxidized MWNTs indicated a 10% resistance decrease when exposed to 1 ppm NO_2 (Fig. 15(a)). This can be explained by the general p-type semiconductor behavior when exposed to the oxidant gas NO_2. NO_2 adsorbs as negatively charged NO_2 (NO^{2-}) on the surface of the MWNTs, as shown in Fig. 17(a), and then hole carriers are injected into the MWNTs, inducing a decrease in resistance. The MWNT-SnO_2 composite sensor shown in Fig. 15(b) shows a decrease in resistance although the MWNTs were apparently completely covered with a few nanometers of SnO_2

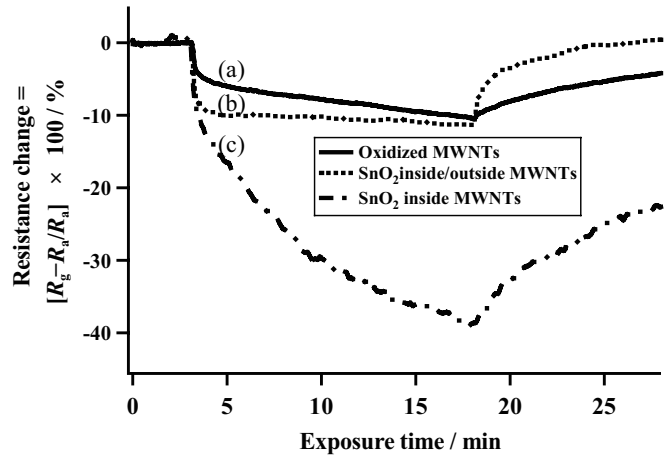

Fig. 15. Response transients of (a) oxidized MWNTs, (b) SnO_2 inside/outside MWNTs and (c) SnO_2 inside MWNTs to 1 ppm NO_2 at 150°C.

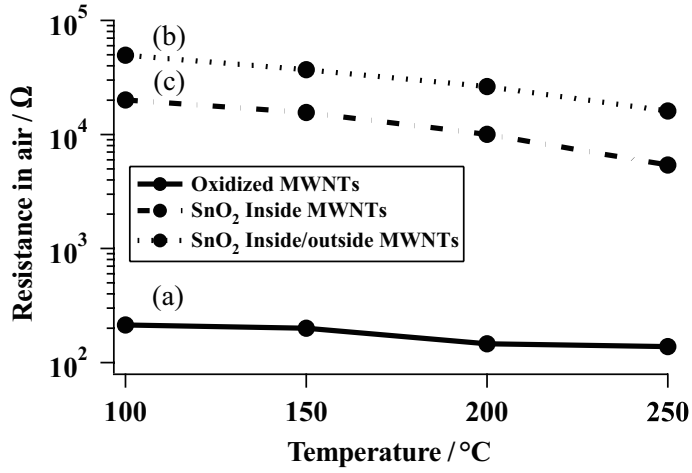

Fig. 16. Temperature dependences of resistance in air of (a) oxidized MWNTs, (b) SnO_2 inside/outside MWNTs and (c) SnO_2 inside MWNTs.

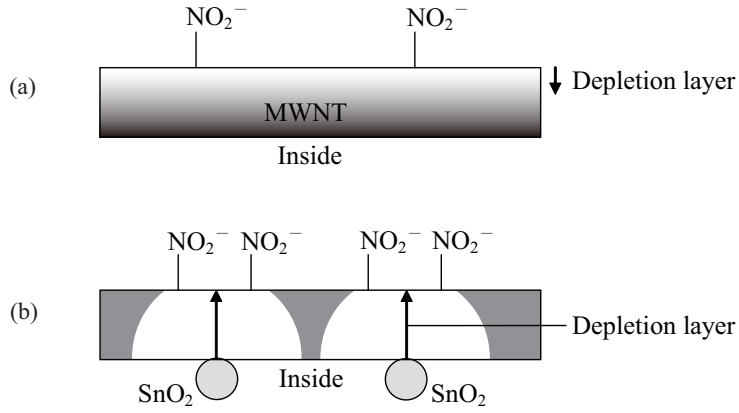

Fig. 17. Formation model of depletion layer in NO_2 adsorption of (a) oxidized MWNT and (b) SnO_2 deposited inside MWNT. A color gradation sequence from white to whitish gray denotes the depletion layer.

nanoparticles, as shown in Fig. 13(a), suggesting a p-type conductive behavior due to the insufficient connection between SnO_2 nanoparticles. In contrast, the MWNTs completely covered with SnO_2 nanoparticles of more than 5 nm in diameter showed an increase in resistance (data not shown in this paper), denoting an n-type conductive behavior when exposed to the oxidant gas NO_2. Figure 15(c) shows the response transient for the composite sensor composed of the SnO_2 nanoparticles of ca. 10 nm in diameter deposited inside the MWNTs, as shown in Fig. 13(c). Interestingly enough, SnO_2 nanoparticles deposited inside the MWNTs indicated the largest resistance decrease of ca. 40% and the longest response time for a NO_2 exposure time of 15 min. Noticeably, the resistance of this composite sensor in air is on the order of 10^4 Ω, as shown in Figs. 16(b) and 16(c), in contrast to that of the oxidized MWNT sensor on the order of 10^2 in Fig. 16(a). This difference in resistance in air depends on the formation of a p-n junction between n-type SnO_2 and p-type MWNTs. The p-n junction contributes to enhanced NO_2 adsorption, similarly to the NO_2 adsorption behavior of the MWNT-WO_3 composite sensor. In the case of the MWNT-WO_3 composite, n-type WO_3 nanoparticles are deposited outside the p-type MWNTs and a p-n junction is formed outside the MWNTs. In contrast, SnO_2 nanoparticles deposited inside the MWNTs form many p-n junctions at connection points between SnO_2 and MWNTs, as shown in Fig. 17(b). The p-n junction contributed to the formation of a large depletion layer beginning on the inner surface of the MWNTs. The depletion layer penetrates the outer part of the MWNTs, and many NO_2 molecules adsorbed on the depletion layer come into contact with to the surface of the MWNTs.

The above modification techniques may be very useful for enhancing the sensing properties of MWNTs to environmental pollution, foul-smelling and volatile organic compound gases.

Acknowledgements

This work was supported by a Grant-in-Aid for Young Scientists (B) (No. 17750136) and a Grant-in-Aid for Young Scientists (A) (No. 19681012) from the Ministry of Education, Culture, Sports, Science and Technology (MEXT). We thank Mr. Takahiro Kishi of Ritsumeikan University for the sensor and HR-TEM measurements of SnO_2-MWNT composites.

References

1 J. P. Lukaszewicz: Sens. Lett. **4** (2006) 53.
2 Q. Fu and J. Liu: Langmuir **21** (2005) 1162.
3 K. S. Ahn, J. H. Kim, K. N. Lee, C. O. Kim and J. P. Hong: J. Korean Phys. Soc. **45** (2004) 158.
4 L. Valentini, F. Mercuri, I. Armentano, C. Cantalini, S. Picozzi, L. Lozzi, S. Santucci, A. Sgamellotti and J. M. Kenny: Chem. Phys. Lett. **387** (2004) 356.
5 J. Li, Y. Lu, Q. Ye, M. Cinke, J. Han and M. Meyyappan: Nano. Lett. **3** (2003) 929.
6 J. Suehiro, G. Zhou and M. Hara: J. Phys. D: Appl. Phys. **36** (2003) L109.
7 L. Valentini, I. Armentano, J. M. Kenny, C. Cantalini, L. Lozzi and S. Santucci: Appl. Phys. Lett. **82** (2003) 961.
8 C. Cantalini, L. Valentini, I. Armentano, L. Lozzi, J. M. Kenny and S. Santucci: Sens. Actuators, B **95** (2003) 195.
9 H. Hu, B. Zhao, M. E. Itkis and R. C. Haddon: J. Phys. Chem. B **107** (2003) 13838.
10 J. H. Lee, J. Kim, H. W. Seo, J. W. Song, E. S. Lee, M. Won and C. S. Hana: Sens. Actuators, B (in press).
11 T. H. Tran, J.-W. Lee, K. Lee, Y. D. Lee and B.-K. Ju: Sens. Actuators, B **129** (2008) 67.
12 H. Q. Nguyen, S. L. Zhang, G. H. Rue and J. S. Huh: Solid State Phenomena **124–126** (2007) 1173.
13 J. Mäklin, T. Mustonen, K. Kordás, S. Saukko, G. Tóth and J. Vähäkangas: Phys. Status Solidi B **244** (2007) 4298.
14 D. H. Nguyen, V. Q. Nguyen, C. Gyuseok, C. Yousuk, Y. J. Se and K. Dojin: Solid State Phenomena **124–126** (2007) 1309.
15 D. H. Nguyen, V. Q. Nguyen, C. Yousuk and K. Dojin: Sens. Actuators, B **127** (2007) 447.
16 R. Ionescu, E. H. Espinosa, E. Sotter, E. Llobet, X. Vilanova, X. Correig, A. Felten, C. Bittencourt, G. Van Lier, J.-C. Charlier and J. J. Pireaux: Sens. Actuators, B **113** (2006) 36.
17 T. Zhang, M. B. Nix, B-Y. Yoo, M. A. Deshusses and N. V. Myung: Electroanalysis **18** (2006) 1153.
18 E. H. Espinosa, R. Ionescu, C. Bittencourt, A. Felten, R. Erni, G. V. Tendeloo, J.-J. Pireaux and E. Llobet: Thin Solid Films **515** (2007) 8322.
19 M. Penza, G. Cassano, R. Rossi, M. Alvisi, A. Rizzo, M. A. Signore, T. Dikonimos, E. Serra and R. Giorgi: Appl. Phys. Lett. **90** (2007) 173123.
20 E. H. Espinosa, R. Ionescu, B. Chambonb, G. Bedis, E. Sotter, C. Bittencourt, A. Felten, J.-J. Pireaux, X. Correig and E. Llobet: Sens. Actuators, B **127** (2007) 137.